metals

MDPI

Article

Cytotoxicity, Corrosion Resistance, and Wettability of Titanium and Ti-TiB_2 Composite Fabricated by Powder Metallurgy for Dental Implants

Ali Mohammad Ali Aljafery [1,2], Abdalbseet A. Fatalla [2,*] and Julfikar Haider [3,*]

[1] Department of Prosthodontic, College of Dentistry, University of Kufa, Najaf 54001, Iraq; alim.aljaafri@uokufa.edu.iq
[2] Department of Prosthodontics, College of Dentistry, University of Baghdad, Baghdad 1417, Iraq
[3] Department of Engineering, Manchester Metropolitan University, Manchester M12 5GN, UK
* Correspondence: abdalbasit@codental.uobaghdad.edu.iq (A.A.F.); j.haider@mmu.ac.uk (J.H.)

Abstract: *Objectives*: Orthopedics and dentistry have widely utilized titanium alloys as biomaterials for dental implants, but limited research has been conducted on the fabrication of ceramic particle-reinforced Ti composites for further weight reductions. The current study compared titanium–titanium diboride metal composites (Ti-TiB_2) with pure titanium (processed by powder metallurgy) in terms of toxicity, corrosion resistance, and wettability. *Methods*: First, cell lines of a primary dermal fibroblast normal human adult (HDFa) were used to test the cytocompatibility (in vitro) of the composite and pure Ti using an indirect contact approach. Corrosion testing was performed for the materials using electrochemical techniques such as potentiodynamic polarization in a simulated bodily fluid (SBF) in conjunction with a three-electrode electrochemical cell. The entire set of experimental tests was conducted according to the ASTM F746-04 protocol. The contact angles were measured during wettability testing in accordance with ASTM D7334-08. An X-ray diffractometer (XRD) was used to catalog every phase that was visible in the microstructure. A scanning electron microscope (SEM) and energy-dispersive X-ray spectroscopy (EDS) were used to determine the chemical composition. *Results*: The cytotoxicity tests revealed that there was no detectable level of toxicity, and there was no significant difference in the impact of either of the two materials on the viability of human fibroblasts. An increase in the corrosion resistance of the composite (0.036 ± 0.0001 mpy (millimeters per year)) demonstrated the development of a passive oxide coating. According to the findings, the composites showed a greater degree of hydrophilicity (contact angle $44.29° \pm 0.28$) than did the pure titanium ($56.31° \pm 0.47$). *Conclusions/Significance*: The Ti-TiB_2 composite showed no toxicity and better corrosion resistance and wettability than did pure Ti. The composite could be a suitable alternative to Ti for applications involving dental implants.

Keywords: biomaterials; dentistry; titanium; titanium diboride; powder metallurgy; cytotoxicity; corrosion; wettability

Citation: Aljafery, A.M.A.; Fatalla, A.A.; Haider, J. Cytotoxicity, Corrosion Resistance, and Wettability of Titanium and Ti-TiB_2 Composite Fabricated by Powder Metallurgy for Dental Implants. *Metals* **2024**, *14*, 538. https://doi.org/10.3390/met14050538

Academic Editors: Yadir Torres Hernández and Khashayar Khanlari

Received: 12 March 2024
Revised: 21 April 2024
Accepted: 26 April 2024
Published: 1 May 2024

1. Introduction

As the aging population around the world is increasing, the use of surgical implants, which involve the replacement of lost or damaged body structures, has emerged as one of the best ways to improve quality of life for these people. Titanium (Ti) is the metal most often used in biomedical engineering because it has great physical and chemical qualities. It is also the most ideal biocompatible material for the industrial production of surgical implants [1,2]. Casting and powder technology are the two primary fabrication methods used for Ti alloys [3].

Dental implants are a popular method for treating tooth loss since they provide both a cosmetic and practical solution. Dental implants are synthetic tooth roots that are surgically inserted into the jaw. Either the mandible or the maxilla can be used to host an implant.

Dental implants connect with bone over time to secure dental prostheses when they are designed and placed correctly. The most frequently used implant materials are titanium and its alloys. However, a new path in implantology has opened up thanks to the great revolution in the fields of ceramics (zirconium dioxide) and polymers (PEEK) as well as other materials [4–8].

The release of titanium and titanium alloy particles and ions into the surrounding tissues as a result of corrosion and wear is a potential problem for dental implants made of titanium. This can lead to bone loss due to inflammatory reactions, and, ultimately, the implant fails to osseointegrate. Yellow nail syndrome is an example of a hazardous reaction that can occur when titanium ions and particles accumulate in other tissues. In addition, hypersensitivity reactions can cause the implant to fail or cause an allergic reaction [9]. In a review of dental implant materials, it was determined that titanium was one of the most poisonous metal ions examined, and that it had an impact on the production of an osteoblast-like phenotype. They acknowledged that it was challenging to extrapolate their findings to the in vivo environment because a dental implant's passivating oxide surface was anticipated to release very little titanium into the body [10]. The development of a dense passive layer on titanium in artificial saliva or in the presence of a 2-day-old *Streptococcus mutans* biofilm indicates that the presence of the biofilm reduces the corrosion resistance of CP-Ti [11]. Despite the widespread use of titanium implants, scientists have never stopped trying to perfect metal alloys with the right balance for maximum biocompatibility and physical strength [12]. Additionally, bone loss may occur if the implant is too close to adjacent teeth [13]. When mixed with other elements, titanium has greater corrosion resistance than commercially pure titanium. The maximum cell viability among Ti alloys—higher than that of CP-Ti—was shown for the Ti-10Nb alloy [14].

Many scientists have adopted the practice of adding reinforcements to titanium to increase its mechanical properties, such as its hardness. Titanium boride (a ceramic material used as a composite with titanium metal) has proven to be an excellent reinforcement material for titanium due to its excellent chemical and mechanical compatibility with the matrix [15–17]. However, little is known about the biocompatibility of these composites, which has prevented their use in biomedical applications, despite the extensive research conducted on them. In addition, there is evidence that the Ti-TiB_2 composite is biocompatible, suggesting that further study is required to determine its potential as a biomaterial [15].

Due to its mechanical and thermal stability as well as the fact that it creates the fewest residual stresses in composites, TiB_2 has recently been found to be the best reinforcement for titanium [16]. Consequently, one of the most desirable titanium matrix composite (TMC) materials is Ti/TiB composites [18]. Numerous studies have been conducted on TiB, not only for grain growth but also to impact α phase nucleation by offering more heterogeneous nucleation sites [19,20]. The α phase that forms from TiB also abides by the orientation relationships of (001) TiB/(0001) α-Ti and [010] TiB/[1120] α-Ti [21]. TiB tends to grow in the [010] direction and has a B27 crystal structure. Since TiB has a hexagonal cross-section and a whisker-like morphology, it may efficiently carry heavier weights due to chemical processes, which can ease interface limits on the distribution of reinforcements [22]. In addition, the incorporation of ceramic materials can increase corrosion resistance [23]. Additionally, it has determined that the thermal expansion coefficient and densities of TiB_2 and Ti are almost identical. During the sintering process, TiB_2 reacts with titanium to produce in situ TiB [17,24].

$$Ti + TiB_2 = 2TiB \quad (1)$$

One of the primary procedures for producing titanium–titanium boride composites is powder metallurgy [25]. Processing in terms of net shape, reduced material waste, and microstructural control is the key advantage of this technique [26]. Selvakumar et al. [27] recently compared the microstructure and properties of Ti-TiBw (whisker) produced by spark plasma sintering (SPS) to those produced by hot isostatic pressing (HIP) and vacuum sintering. The TiB_2 was mostly transformed to fine TiBw whiskers only in the spark-

plasma-sintered products. This is not unexpected given that it has been demonstrated that electric current has an inherent effect that accelerates diffusion and phase change dynamics [28]. Recent studies have investigated forging Ti-TiBw and Ti-TiBw hybrid composites for bulk deformation processing (BDP) [29], extrusion [30], equal-channel angular pressing [31], and hot rolling [32]. Although there has been much research on traditional constituent mixing techniques, such as casting or powder metallurgy processing, only a few studies have investigated alternate designs [25,28]. Numerous studies have investigated the production of Ti-TiBw composites using additive laser sintering. A review by Attar et al. is recommended to the reader for providing a thorough understanding of this research area [33]. Additionally, Ti-TiBw has been discussed as a potential biomaterial and needs further investigation [34].

Sintering aids are typically required to promote liquid-phase sintering because it is difficult to sinter TiB_2 at full density. Nickel boride, iron, and SiC have all been tested as additives [35]. A density greater than 94% was attained by Einarsrud et al. [35] when employing 1700 °C pressure-free sintering. Grain growth was enhanced by the addition of Ni and NiB and ranged from 3 to 20 μm. The ductility of the TiB-reinforced Ti composites is a key concern. At room temperature, composites with a TiB addition of more than 30% showed no ductility. As the amount of TiB increased, the brittleness also increased. For composites made of Ti/TiB_2, the same issue occurred. At high temperatures, Ti, β phase, and TiB composites manufactured from titanium powders, such as titanium alloyed with Fe-Mo, Mo, and/or Nb [36], possess substantially better ductility. The TiB_2 concentration had a significant impact on the mechanical and physical characteristics [37]. Even at high sintering temperatures and especially in the absence of a β stabilizer for Ti, excessive amounts of highly hard TiB_2 can cause noticeable cracking in specimens that undergo spark plasma sintering at 850 °C [38]. Therefore, using high titanium diboride concentrations without a β stabilizer is not recommended, and this is supported by a number of studies [39,40].

TMCs can be produced using standard casting methods as well as powder metallurgy (PM) methods. In contrast, PM successfully prevents casting flaws, such as coarse microstructures, shrinkage holes, and segregation, while also increasing productivity. It also allows for near-net manufacturing of components with complex geometries and offers good control over determining the final performance of TMCs [41].

Certain conditions are necessary for successful compatibility between the biomaterial and tissue, including the physicochemical interface phenomena related to the first contact between the biomaterial, tissue, and implantation environment; the response of the tissue and organic medium to the presence of the material; changes in the materials as a result of the medium's (tissue, organic fluids) action, degradation, and corrosion; and the reaction of a part of the organism not typically exposed to the biomaterial [42]. The wettability is correlated with the surface energy of the solid material. An increased surface energy of the solid material results in enhanced wettability and a reduced contact angle. The contact angle is influenced by both the surface roughness and surface phase [43].

While Ti implants are frequently utilized in dental implant procedures, their effectiveness is contingent upon the quality and amount of bone. However, existing research does not provide any comparison between Ti implants and the created $Ti\text{-}TiB_2$ composite. Moreover, there has been limited research on TiB_2, especially in the context of dental implants. Dental implants need to have the right level of porosity to promote bone integration and should also be lightweight to prevent implant fracture while still maintaining high strength for successful chewing. In general, ceramic materials have high porosity and simultaneously possess excellent mechanical properties [44]. This explains why the presence of these titanium diboride materials (especially titanium bride whiskers, TiBw) that cause porosity when forming a composite with titanium metal does not negatively affect the mechanical properties.

The objective of this study is to produce durable and lightweight dental implants that are compatible with the human body. This goal will be achieved by analyzing the toxicity to cells, corrosion properties, and ability to attract water (hydrophilicity) of dental implant

composites made from titanium and titanium diboride compared to pure titanium by powder metallurgy processing. The results will provide insights into how these composites interact with biological systems.

2. Experimental Methods

2.1. Main Materials

Both titanium (Ti) and titanium diboride (TiB_2) powders were purchased from the Chinese company Hangzhou Hyper Chemicals Limited for use in this research. The average particle size of the pure Ti powder was approximately 20 µm, and the TiB_2 particle size was 10 µm.

2.2. Powder Metallurgy Procedure

2.2.1. Mold Details

The mold was made from stainless-steel materials and consisted of four parts: a die, two bases, and a punch (Figure 1). The die was a hollow cylinder measuring 50 mm in height, with an inner diameter of 12 mm and an outer diameter of 18 mm. The first base was a disc 15 mm in height by 22 mm in diameter; at the center of the base was a short, solid rod, 5 mm in height by 11.5 mm in diameter. This rod was inserted inside the hollow space of the die when it was seated on the base while pressing the powders. The second base was a hollow cylinder (35 mm height × 20 mm top inner diameter) with a 30 mm outer diameter; at 2 mm hollow depth from the top end, there was a shoulder (3 mm width), so the inner diameter decreased to 14 mm at the beginning of the shoulder. The die was placed on this shoulder after pressing to facilitate ejection of compacted samples. The punch rod used had the following dimensions: 11.5 mm in diameter and 75 mm in height. A rod was used for the compaction of powders inside the die and for ejecting the specimen outside the die.

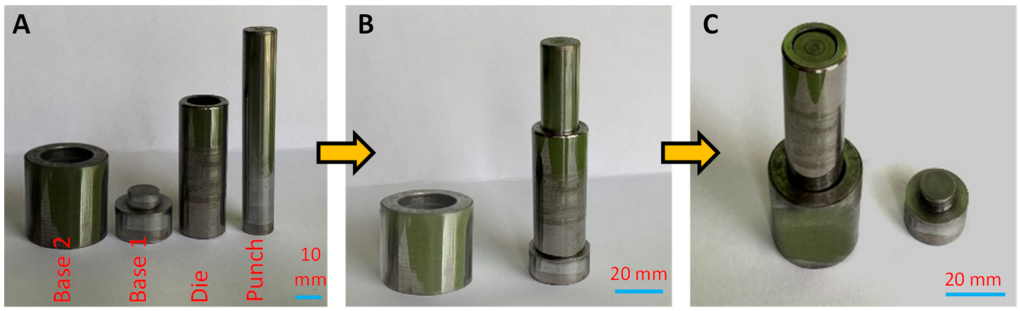

Figure 1. (**A**) Parts of the mold, (**B**) pressing powder position, (**C**) sample removal position.

2.2.2. Powder Preparation

Two sets of specimen powders were made, one from pure titanium (Ti) and the other from Ti and 9 wt.% titanium diboride (Ti-TiB_2). Approximately 20 h of dry ball-milling (pure and composite) was carried out in a planetary ball mill (MSK-SFM-1, MTI Corporation, Richmond, CA, USA). When mixing, stainless-steel balls outweighed the powder by a factor of 10. For further processing, the milled powder was kept under vacuum [45].

2.2.3. Sample Preparation (Cold Compacting)

Samples for the cytotoxicity, corrosion, and wettability tests, in accordance with ISO 10993-5, ASTM F746 04, and ASTM D7334-08 [46–48], were all manufactured with an 8 mm height and an 11.5 mm diameter. Ten samples each from the two materials were created for each test. Powder (3.5 g) was weighed to make green specimens, which were placed in molds and pressed uniaxially with an electronic hydraulic press controlled by a digital gauge (Carver, Gardena, CA, USA) at a pressure of 800 MPa to obtain a green density of 3.151 g/cm^3.

2.2.4. Consolidation (Vacuum Sintering)

The temperature for sintering must be at least 0.7-times the melting point of the material [49]. In a vacuum tube furnace (less than or equal to 0.1 MPa), cylindrical green composite (compacted and unsintered powder particles that are held together by mechanical pressure) powder billets were sintered (Lanphan SK2, SK2-7-14TPD3, Henan Lanphan Industry Co., Ltd., Zhengzhou, China) for 5 h at 1200 °C. TiB_2 and titanium powder reacted during the sintering process to create TiB [45]. Although Ti_3B_4 is typically generated at temperatures greater than 1900 °C, it is possible that it could be a TMC intermediate phase, according to some speculation [24,50]. The Ti_3B_4 phase was not considered in this study because the sintering temperature was 1200 °C.

2.3. Microstructural Characterization

The microstructures and elemental makeup of the pure and composite materials were examined using SEM and EDS, with an average working distance (WD) of 11.5 mm and a voltage of 25–30 kV (Inspect S50, FEI Company, Eindhoven, The Netherlands). The Ti and TiB phases in the composites after sintering were confirmed via XRD (Shimadzu, XRD-6000, Kyoto, Japan). CuKα radiation was used for the XRD analysis of metallographically polished samples at 40 kV and 40 mA between 30° and 80°.

2.4. Cytotoxicity Test (Cell Metabolic Activity Evaluation, MTT Assay)

2.4.1. Sample Preparation

The surfaces of the samples that were prepared for this test were washed and submerged in a solution of HNO_3 (9%), HF (5%), and deionized water for 30 min prior to cytotoxicity testing. The primary goal of using this technique was to remove any surface products that may have formed during processing. For instance, the accumulation of titanium oxide on sample surfaces and other substances could skew the findings of cytotoxicity tests [51].

2.4.2. Culture of Cells (Cell Lines)

The primary dermal fibroblast normal, human, adult (HDFa), and PCS-201-012TM cells utilized in this study were donated by the American Type Culture Collection (ATCC, Rockville, MD, USA). The cells were grown in Dulbecco's modified Eagle medium (DMEM), supplemented with 10% fetal calf serum (FCS), penicillin (100 U/mL), streptomycin (100 mg/mL), and amphotericin B (2.5 g/mL) under standard conditions. The cells were incubated at 37 °C in a water-saturated atmosphere with 5% CO_2. The cells were removed from the culture bottles before they formed a confluent monolayer by incubating them with a 0.25% buffered trypsin solution under the recommended conditions. After every 4 days, new media were added to the cultures. The concentration of the cell suspensions and the viability were evaluated using Trypan Blue staining and a Neubauer chamber. To adjust the cell concentrations, fresh medium was added, and 1×10^5 cells were planted into each well of a 96-well plate. The cells were allowed to stabilize for 24 h under normal conditions before the experiments [52].

2.4.3. Indirect Mode of Contact

The pure samples (Ti), composite samples (Ti-TiB_2), high-density polyethylene film (the negative control), and polyurethane film with 0.1% zinc diethyldithiocarbamate (ZDEC) (the positive control) were all sonicated in neutral soap at 15% before being tested for cytotoxicity. Following a deionized water wash, the samples were sonicated in benzalkonium chloride for 15 min (1:10). The samples were all sterilized in an autoclave at 120 °C for a total of 15 min. According to the ISO 10993-5 protocol, an in vitro cytotoxicity test (indirect contact method) was carried out [46]. The materials were submerged in complete culture medium for 1, 2, 3, or 5 days to obtain the extracts eluted from the samples into the culture medium. The pure Ti and composite materials were extracted at a ratio of 20 mL per 60 cm^2, whereas the negative and positive controls were extracted at a ratio of 120 mL per 60 cm^2.

The extracts containing each material's degradation products were then collected after 1, 2, 3, and 5 days, and all the extracted materials were stored in an incubator at 37 °C for 24 h for each period. The medium containing the leachate was removed at the end of each incubation (4 times) and used for the cytotoxicity test, presuming it to be 100% leachate. Fresh media were diluted exponentially with the leachate medium. In a 96-well plate that had previously been seeded with HDFa cells and stabilized for 24 h, nine serial dilutions were generated. Then, 100 µL of each leachate dilution from the pure and composite materials, as well as from zinc diethyldithiocarbamate (ZDEC) and high-density polyethylene, was added. The plates were then incubated for an additional 24 h at 37 °C and 5% CO_2 [53]. The plates were once more incubated for 4 h, as per standard procedures, after the leachate medium from each well was removed and replaced with 100 µL of a solution of 3-(4,5-dimethyl-thiazol-2-yl)-2,5-diphenyl-tetrazolium bromide (MTT) (1 mg/mL) in a new culture medium. Aspiration was used to carefully remove the medium without removing the formazan crystals after they had been broken down with Dimethyl sulfoxide (DMSO). The absorbance of each substance was calculated using a UV–visible spectrophotometer (UV-1900, Shimadzu, Kyoto, Japan) at a wavelength of 540 nm. Equation (1) was used to calculate the percentage of live cells:

$$percent\ of\ viable\ cells\ \% = \frac{ABS_s}{ABS_c} * 100 \quad (2)$$

where ABS_c is the average value of the negative control (100%) and ABS_s is the value of the absorbance for each sample.

2.5. Corrosion Resistance Test

To test the corrosion of previously manufactured specimens in a simulated body fluid (SBF) solution with a pH of 7.4 at 37 °C and to assess how the pure titanium and composite dental implants react to the body, Table 1 provides information on the chemical makeup of the SBF [54]. SBF, which is similar to all body fluids, was used for the corrosion tests because the dental implants considered here are in direct contact with the jaw bones, blood, and body fluids rather than the saliva in the oral cavity. One of the methods for evaluating corrosion behavior in SBF solution is electrochemical potentiodynamic polarization [55], and according to ASTM F746-04 [47], electrochemical tests of the samples were conducted using an electrochemical workstation (CS2150M Bipotentiostat, CORRTEST Instruments, Wuhan, China). For electrochemical measurements, a standard three-electrode cell system was employed, consisting of a platinum electrode acting as the counter electrode (CE) and a saturated calomel electrode (SCE) serving as the reference electrode, and a disc sample working electrode was created from the test materials by machining, grinding, and recommended final polishing using 600-grit metallographic paper, with an exposed area of 1 cm^2, according to ASTM F746-04. A potential range of −0.3 V to 0.8 V was used for potentiodynamic polarization testing and the corrosion potential ($E_{coor.}$) at the open circuit potential (OCP) after obtaining a stable OCP value at a scanning rate of 1 mV/s. According to the procedure outlined in a prior work, the linear polarization resistance (LPR) of the samples was evaluated in a potential scan range of 20 mV vs and OCP with a potential rate of 10 mV/min [56]. The corrosion test in the SBF solution produced corrosion test parameters such as the corrosion current density (I_{corr}.) and corrosion rate (CR). Equation (2) provides the measurement of the corrosion rate [57].

$$CR = \frac{0.13 * Icorr * E_w}{\rho} \quad (3)$$

where I_{corr} is the corrosion current density (µA/cm^2), E_W is the equivalent weight (g/eq.), ρ is the density (g/cm^3), and 0.13 is the metric and time conversion factor.

Table 1. Composition of simulated body fluids, SBF (mmol/L) [58].

Ions	Na^+	K^+	Mg^{2+}	Ca^{2+}	Cl^-	HCO_3^-	HPO_4^{2-}	SO_4^{2-}	Buffer	pH
SBF	142.0	5.0	1.5	2.5	147.8	4.2	1.0	0.5	Tris	7.4

2.6. Wettability Test

Surfaces of both types of samples were prepared to achieve a similar roughness value of 1.5 ± 0.5 µm to avoid any bias from the roughness on the contact angle measurements. With the use of a measurement apparatus for optical contact angle (Kino, SL200KS, Solon Tech, Shanghai, China), the wettability angle was calculated. The apparatus, based on a multi-axis positioning sample stage, used a micrometer, an automatic direct syringe pump with an accuracy of 0.001 mm, 0.9 mm outer diameter stainless-steel needles, and a highly accurate optical vision system. The SBF solution was utilized for the wettability test.

The manufacturer's software and a digital microscope were used to calculate the contact angle. According to ASTM D7334-08 guidelines, the needle was positioned 3 mm from the substrate, the 20 µL drop limit was controlled by a micrometer, and three drops were applied to the samples. The contact angles on the two sides of the drops were measured to determine the average of the three drops [59]. The wettability angles of the test substrates are shown in Figure 2. The drop is depicted in the picture, and both sides of the drop angle are shown. Twenty seconds after the drop and deposit, images were taken. The samples were cleaned with water and neutral soap and sonicated for 15 min to remove organic pollutants [60].

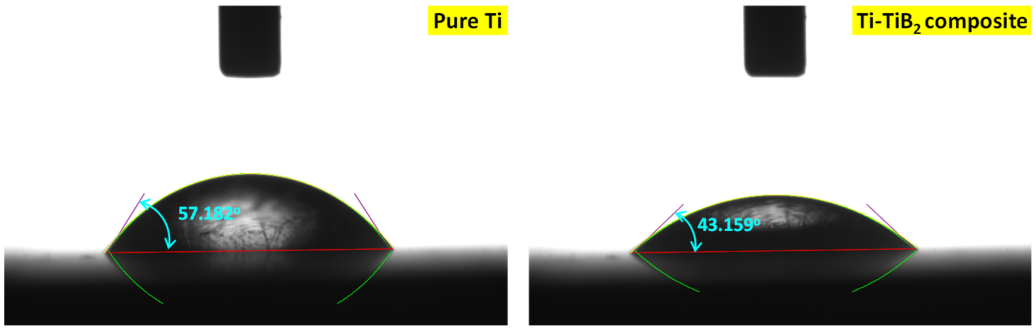

Figure 2. Examples of the wettability angles of the pure (Ti) and composite (Ti-TiB_2) samples.

2.7. Statistical Analysis

By using GraphPad Prism version 9, the results were analyzed with appropriate statistical techniques, including, first, descriptive statistics (box plot) and, second, inferential statistics (unpaired t test) to test the significance of the mean values (p value < 0.05).

3. Results and Discussion

3.1. Composite Sample Characterization

Figure 3 shows the characteristic XRD patterns of the samples. The presence of α-Ti peaks in the diffractogram patterns of the composites indicates that the sintering process was complete. The findings also showed that Ti_3B_4, a potential intermediary phase in the matrix, did not exist [61]. This observation also shows that in the matrix, the TiB_2 particles transformed into TiB. Additionally, the XRD pattern of the composite reveals a single TiB_2 peak (111) at 2θ = 68.326°. This is consistent with the findings of an earlier investigation and points to the slow diffusion of boron atoms in TiB [45,62]. In contrast to the pure sample peaks of α-Ti, the composites show prominent TiB (200 and 113) peaks. All the composite samples had the same phase composition, with α-Ti and TiB being the two most conspicuous phases in all composites.

This outcome was in line with the findings of Namini and Azadbeh [39], who noted the presence of Ti, TiB, and TiB_2 phases in the X-ray diffraction pattern of a Ti-TiB_2 sample. The

in situ reaction between Ti and TiB_2 and the creation of the TiB phase were supported by the TiB diffraction peaks that were observed in the XRD pattern. In direct contact, TiB_2 and Ti are thermodynamically unstable and react to form TiB when there are too many moles of titanium present, according to research on the Ti-TiB_2 sintering process [30]. Additionally, the weak TiB_2 peaks that coexisted with the Ti and TiB diffraction peaks demonstrated that at this sintering temperature (1200 °C), the vacuum sintering process did not entirely complete the chemical reaction between Ti and TiB_2.

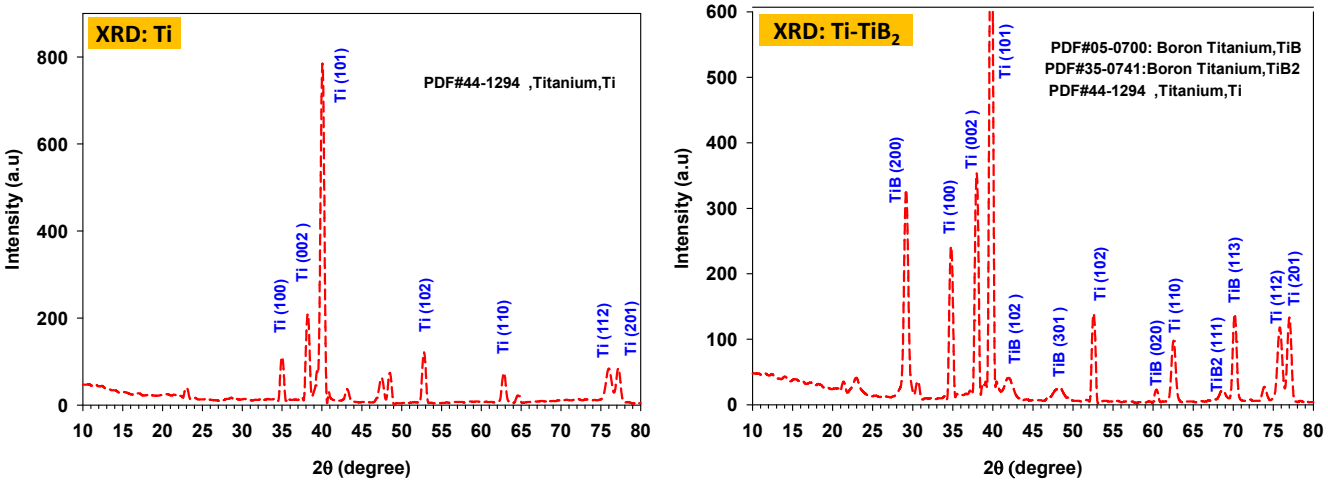

Figure 3. XRD patterns of pure (Ti) and composite (Ti-TiB_2) samples.

The EDS results for the composite and pure samples are displayed in Figure 4. The results supported the distribution of Ti and boride phases in the composite. The picture depicts two different zones independent of porosity with a color map of titanium (green) and boron (yellow) in the composite samples. There was a dark-gray boride-rich region that was primarily composed of titanium boride (TiB), while the other regions were light gray, confirming the presence of titanium. However, it was conceivable that a few whiskers of titanium-boron (TiB) could have formed in the titanium outer matrix due to boron atoms diffusing to the Ti-rich regions during the sintering procedure. In contrast, the pure sample was completely light gray (green color map), with a dark area of porosity and a darker line of crystalline borders. Additionally, as shown by EDX spectroscopy, very little oxygen was present in both groups during processing. The homogeneous distribution of B in the analyzed region shows that the diffusion of this element was adequately completed by the sintering process. The analyzed region appeared to be in the TiB phase based on the concentration of Ti and B.

After the samples had been ground, polished, and deeply etched (using Kroll's reagent), high-magnification SEM images were taken in SEI mode to show the distribution of the TiB whiskers; the sample preparation procedure for SEM was in accordance with ASTM E407-07, and the metallography and microstructures of titanium and its alloys were obtained [63,64]. Figure 5 shows how the TiB whiskers are distributed across the composites. Short whisker clusters, needle-shaped whiskers, and fine TiB plates are observed. The needle describes the morphology of the TiB particles, which have a rod-like form. The crystal structure of TiB can impact the creation of a needle-like morphology. Clusters refer to densely packed assemblages of TiB whiskers. These clusters can arise as a result of several factors, such as intense plastic deformation, sintering heat, or other processing procedures. Plate morphology refers to the form and measurements of the whiskers, without consideration of any particular material or characteristic. The composite appeared to have a homogeneous distribution of interconnected short agglomerated TiB whisker clusters. Such collections of brief TiB whiskers were reported in earlier research [45,61]. The homogenous titanium sprouted into a few long TiB whiskers versus a pure sample of only homogeneous titanium, devoid of another TiB phase.

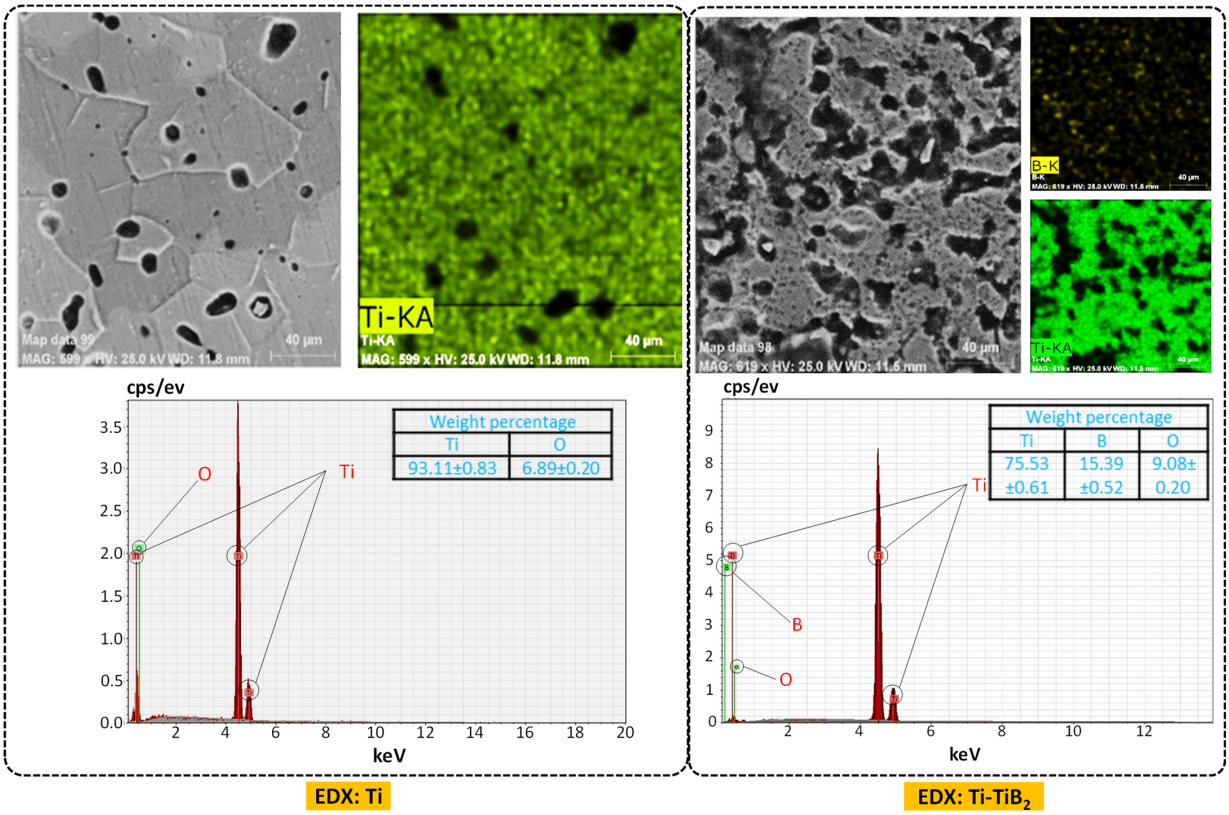

Figure 4. EDX of pure (Ti) and composite (Ti-TiB_2) samples.

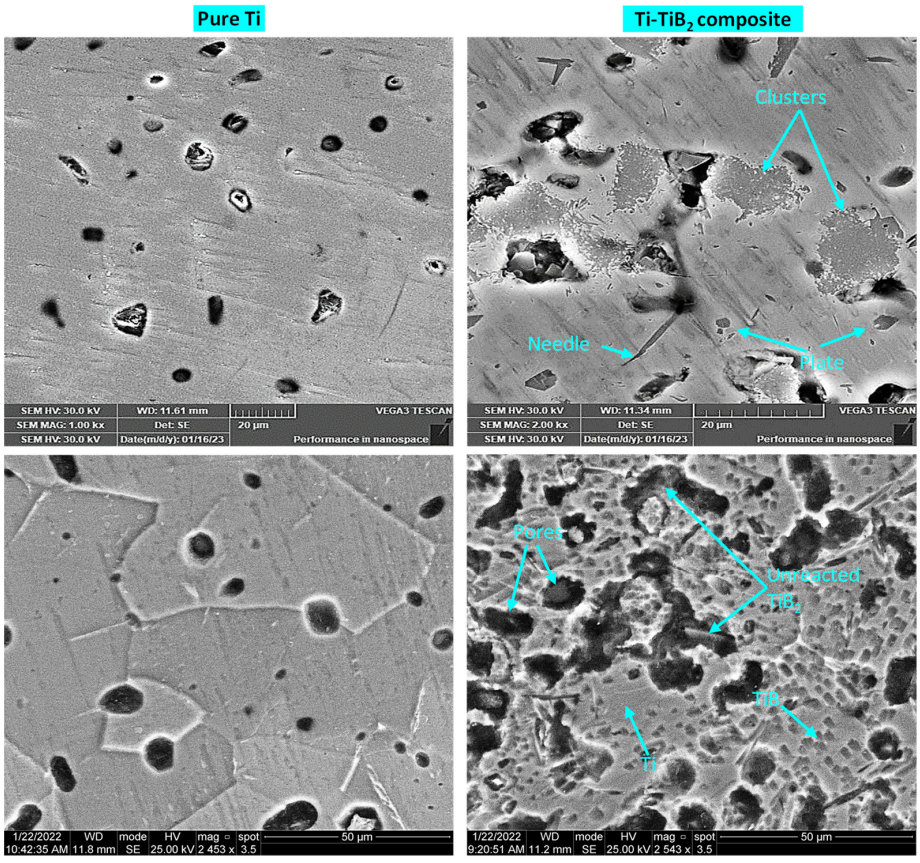

Figure 5. Scanning electron microscopy (SEM) images of both pure titanium (Ti) and composite titanium–titanium diboride (Ti-TiB_2) samples at two different magnifications.

SEM images of the composites revealed three distinct colors: Ti (light gray), TiB_2 (black), and TiB (dark gray). Random TiB whiskers were present on the polished sample surfaces (Figure 5). Additionally, the SEM images clearly depict the unreacted TiB_2 particles, suggesting that the reaction between TiB_2 and the matrix material was not complete, which was in agreement with the previously mentioned XRD findings. There were numerous pores at the location where the reinforcement and matrix met. According to earlier research [39], it is probable that titanium consumption by TiB_2 particles during the chemical reaction between Ti and TiB_2 caused a volume reduction, which, in turn, led to the development of pores.

On the other hand, the pure Ti microstructure at higher magnification shows grains with grain boundaries, and the dark areas indicate pores. At lower magnification, the Ti matrix shows darker pores, but the grains are not visible.

3.2. Cytotoxicity Test (MTT Assay)

Based on the statistical evaluation of the MTT assay results shown in Figure 6, the line of cells (HDFa) used was resistant and tolerant to all leachate levels in both the pure titanium material and composite materials at all incubation times (1, 2, 3, and 5 days), whereas the values of cell viability ranged from 80% to 95%, with an average of 88.35% ± 3.27% pure and 88.64% ± 3.15% composite for overall concentrations and incubation times (all values > 70%). Additionally, during the 1- and 2-day incubation periods, there were no statistically significant changes between the investigated materials (pure and composite), where the average cell viabilities of the composites after 1- and 2-day incubation were 94.54% ± 0.045 and 91.73 ± 0.047, respectively, and for pure Ti, they were 94.52% ± 0.09 and 91.71 ± 0.037, respectively (p value 0.8, t = 0.2 of 1 day, and p value 0.7, t = 0.33 of 2 days) according to the unpaired t test. The investigated materials (pure and composite) showed statistically significant changes after 3 and 5 days of incubation, where the average cell viabilities of the composite after 3 and 5 days were 88.29% ± 0.05 and 79.99 ± 0.03, respectively, and those of the pure composite were 87.68% ± 0.035 and 79.49 ± 0.032, respectively ($p < 0.0001$, t = 9.878 after 3 days, and $p < 0.0001$, t = 10.99 after 5 days), according to the unpaired t test.

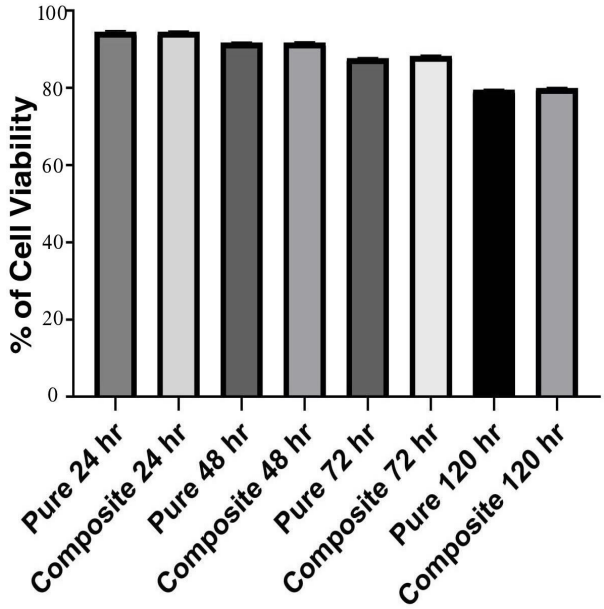

Figure 6. Bar chart showing the cytotoxicity (MTT assay) of the pure (Ti) and composite (Ti-TiB_2) materials at different time intervals. Note: Error bars are present but cannot be clearly observed because the values are very small.

On the other hand, leaching of the positive control (polyurethane film with 0.1% zinc diethyldithiocarbamate (ZDEC)) caused considerable cell death at a 15.5% leaching concentration. Similar cytotoxicity results have been reported for this composite, which is classified as a biomaterial [15,65].

Based on the findings of this study, titanium–titanium boride composites have great potential for use in the biomedical field; however, more research is needed to establish their strong cytocompatibility. Titanium composites, such as Ti-TiBw and Ti-TiC, have demonstrated significant improvements in wear resistance compared with Ti. Additionally, according to several studies (discussed in the corrosion section of this study), it may be possible to take these composites into account for such applications to improve corrosion resistance.

To clarify, the MTT test is commonly used to investigate the cytotoxicity of compounds such as TiO_2 and pure titanium. Cell viability is dose-dependently affected by TiO_2, with certain cell lines undergoing substantial cytotoxicity. In one study, TiO_2 was cytotoxic to HT29-MTX-E12 cells after 24 h but not to Caco-2 cells [66]. Other investigations have shown that TiO_2 can boost osteoblast MG63 cell growth and proliferation without causing malfunction [67]. Research has demonstrated that pure titanium does not have notable cytotoxic effects on cells, in contrast to other alloys such as Ag-Pd and Ni-Cr [68].

Clinical tests of the biocomposites developed in this work are foreseen. As a first step, this procedure was carried out on rabbits, and positive results were obtained.

3.3. Corrosion Resistance (Potentiodynamic Polarization)

The mechanisms for implant-induced ion release into the body include corrosion and surface-layer deterioration. Excessive metal ion leakage from body implants in humans can have negative biological effects and can result in mechanical failure of the equipment. It is widely acknowledged that the homogeneity of the passive layer on the metal surface has a significant impact on the biocompatibility, corrosion resistance, and corrosion rate of these materials. A significant passivating oxide layer naturally forms on the surface of titanium. In most cases, the passive coating on titanium has a thickness of 2–5 nm. Ti has occasionally been detected in tissue around implant prostheses, despite conforming to its metal substrate and having the ability to swiftly regenerate after being weakened. The main structural component of the Ti oxide layer (rutile) is TiO_2. By adding specific elements to the surface oxide layers and naturally stabilizing them, the corrosion resistance of Ti alloys can be enhanced [69]. Additionally, the composition of the porous layers mostly consists of rutile, anatase, and TiB. The presence of stable rutile TiO_2 enhances the chemical stability of the oxide layers, whereas the presence of TiB is attributed to its exceptional catalytic capabilities [70]. The enhanced corrosion resistance observed in the presence of oxide or ceramic materials can be primarily due to their ability to serve as stable barriers, effectively impeding the movement of corrosive ions toward the substrate [71].

While titanium quickly forms an oxide layer in air or in natural tissue fluids due to its membership in the solid reactive metal group, it has a rapid passivation rate [72]. Because titanium and titanium alloys are implanted inside the human body, which is a liquid environment, SBF was chosen as a solution for assessing the corrosion behavior of titanium and titanium alloys. The $E_{corr.}$ of the OCP began to shift in a positive direction as the immersion time increased, and it continued to change positively until it reached a value that was almost steady. The $E_{corr.}$ of the OCP values of the Ti–TiB_2 composite increased as the amount of TiB_2 increased. The OCP level decreased over the course of the experiment, and it showed spikes that corresponded to abrupt fluctuations that were indicative of a corrosive attack from the environment on the exposed surface. Variations in OCP were then followed by a potential stability that was the result of a balance between the attack on the oxide coating and its repair. Potentiodynamic polarization was used to study the corrosion behavior of Ti and Ti–TiB_2 composites in SBF solutions. The goal of this research was to estimate how materials behave when exposed to corrosion. A tabular representation of the corrosion parameters can be found in Table 2.

Table 2. Corrosion current density ($I_{corr.}$), corrosion potential ($E_{corr.}$), and corrosion rate of the tested materials.

Samples	$I_{corr.} \times 10^{-3}$ mA/cm^2	$E_{corr.}$ mV	Corrosion Rate mpy (Millimeter per Year)	Cathodic Tafel Slope β_c	Anodic Tafel Slope β_a
Pure (Ti)	0.215 ± 0.0019	−84.8 ± 0.46	0.084 ± 0.0011	−54.5	36.9
Composite (Ti-TiB_2)	0.066 ± 0.0015	4.5 ± 0.094	0.036 ± 0.0001	−33.6	28.6

It is evident from Table 2 and Figure 7 that the corrosion resistance of the composite significantly improved ($p < 0.0001$, t = 42.81) according to the unpaired t test. The average I_{corr} for the composite specimens was 0.066 μA/cm^2, which is less than the I_{corr} for pure Ti, which is 0.215 μA/cm^2. The E_{corr} value for the composite (4.5 mV) was greater than the E_{corr} value for pure Ti (−84.8 mV); consequently, the composite became more noble.

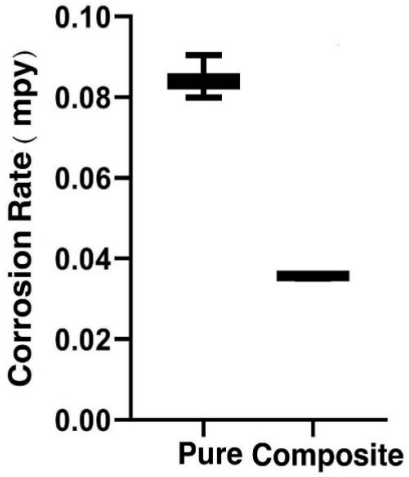

Figure 7. Box plot of corrosion rates for pure (Ti) and composite (Ti-TiB_2) materials.

The polarization curves for the pure Ti and Ti-TiB_2 composites in the SBF solution are shown in Figure 8. With increasing corrosion potential during cathodic polarization, the corrosion current decreased until it reached its lowest feasible level. The extent of corrosion during anodic polarization increased as the active anodic polarization increased [73]. The specimens that are more prone to passivation, however, must undergo a number of active–passive transitions. Consequently, the protective layer of the submerged specimen must be suitably integrated [74].

However, it is worth noting that the corrosion behavior was influenced by the alignment of the TiBw in relation to the test surface. In this study, it was shown that when titanium boride whiskers (TiBw) were oriented perpendicular to the surface, there was a reduction in the exposed planar area of the TiBw. Consequently, this orientation led to a decrease in the galvanic effect compared to that of TiBw, which was aligned parallel to the surface [34].

In light of the behavior of TiB_2, it is necessary to conclude that during the composite's immersion and anodic polarization in the SBF solution, the passivation was controlled by the creation of Ti oxide and was further accompanied by the oxidation of Ti with the boron of TiB_2 at the composite surface. It might either be incorporated into the passive film or produce soluble TiB_2 species. The corrosion stability of Ti-TiB_2 seems to make it appropriate for implant applications.

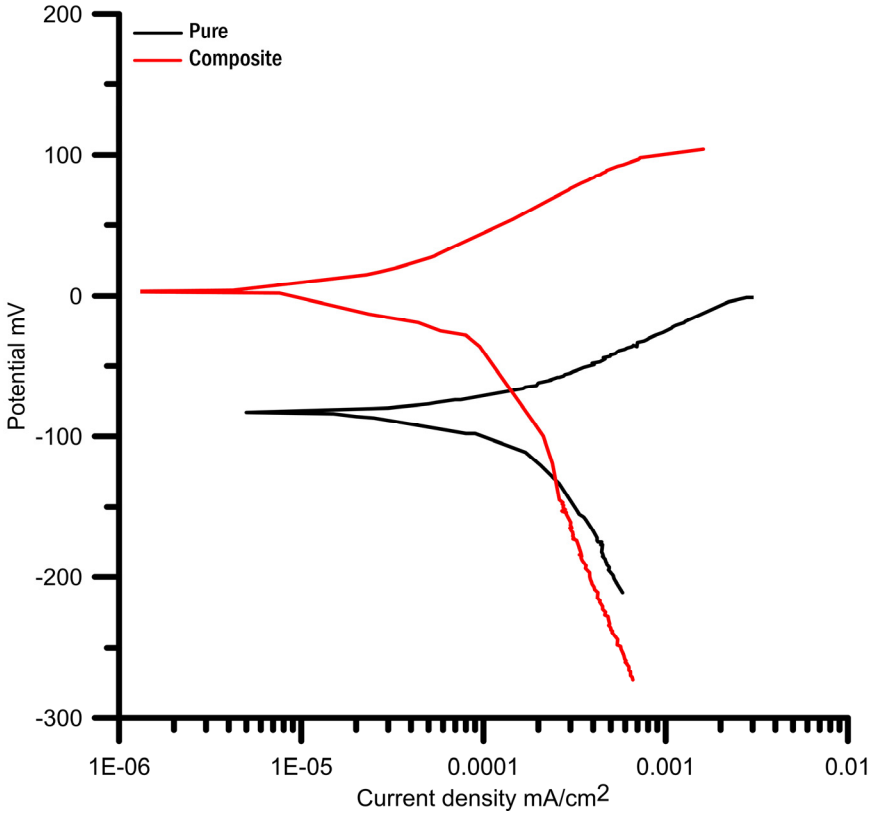

Figure 8. Comparison of potentiodynamic polarization curves in SBF for pure (Ti) and composite (Ti-TiB_2) materials.

3.4. Wettability Test

The average wettability angles for the pure and composite samples were 56.31° ± 0.47 and 44.29° ± 0.28, respectively, showing that the surface of the composite was more hydrophilic. According to the unpaired t test, Figure 9 shows that the composite's wettability significantly improved (p = 0.0001, t = 21.87). The hydrophilicity of a substance, which is associated with surface energy, directly affects how it interacts with proteins, cells, and microbes. These interactions, in turn, have an impact on how well the implants osseointegrate [75]. The hydrophilicity of the surface increased with a decreasing contact angle. If the contact angle produced between the surface and the drop is smaller than 90° when the liquid drop angle is measured, this surface is defined as hydrophilic; otherwise, it is hydrophobic [76]. Greater cell adhesion on hydrophilic surfaces promotes osseointegration [77]. All of the samples in this investigation were hydrophilic according to this measurement. The composite's contact angle of 44.29° indicated that it was more hydrophilic than the pure component. The interaction between cells and the surface of a biomaterial can be influenced by a number of factors, not least hydrophilicity.

Surrounding tissues are impacted by dental implant surface alterations and altered hydrophilicity, although the in vivo molecular mechanisms by which this occurs are inadequately known. According to research by Roach et al., fibrinogen binds more strongly to hydrophobic surfaces in vitro, and proteins adsorbed onto these surfaces have a less well-defined secondary structure [78].

Xi examined how interactions between molten Ti-Al, Ni-Al, and Ni-B alloys and TiB_2 affect the wettability of the alloys. Ti-Al alloys in molten form exhibited excellent wetting of the TiB_2 ceramics. At the Ti/TiB_2 interface, a homogeneous TiB layer developed, whereas a layer of tightly packed TiB whiskers was observed at the contact of the Ti-Al/TiB_2 couple. Generally, the increased porosity of composites due to the addition of TiB_2 reinforcement leads to more liquid being attracted to these pores, and the ceramic material (TiB_2) has good hydrophilic properties, increasing the wettability of composites over pure Ti [79].

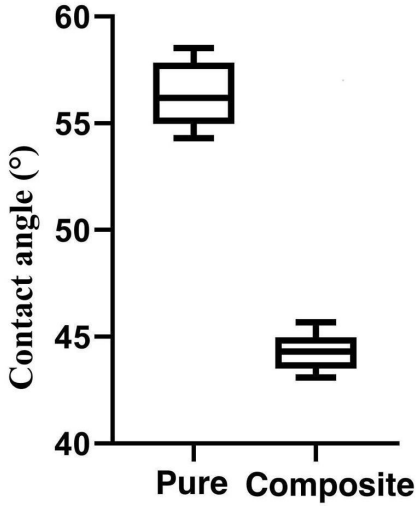

Figure 9. Box plot of wettability for pure (Ti) and composite (Ti-TiB_2) materials.

Generally, the increased porosity of composites due to the addition of TiB_2 leads to more liquid being attracted to these pores [80], and the ceramic material (TiB_2) has good hydrophilicity, which increases the wettability of the composite over that of pure Ti. Sandblasting and acid etching of Ti implant surfaces were suggested as effective techniques to create a favorable surface, which helps to integrate the implant with soft and hard tissues [81]. The adhesion energy between contacting cells can be deduced from the geometry of the contact and the interfacial tensions at the solid–liquid, liquid–vapor, and solid–vapor interfaces [82]. Therefore, a lower contact angle increases the hydrophilicity of the surface and eventually leads to increased cell adhesion.

Composites with high free energy also have high corrosion resistance, as shown in Figure 8 (corrosion resistance and surface energy relation). In contrast, the corrosion resistance of the (pure) samples that showed lower free energy decreased, contradicting the findings of Dos Santos Monteiro et al. [83]. The disparities between the alloying system and the composite system (metal Ti with ceramic TiB_2) could be attributed to this. Chemical reactivity, which is promoted by an energetic surface and results in a higher susceptibility to chemical oxidation passivity, can be used to explain this behavior. The composite is advantageous from this perspective because of its increased hydrophilicity, decreased toxicity, and increased corrosion resistance for real-world dental implant applications.

4. Conclusions

The findings of this study allow us to draw the following conclusions:

1. The Ti-TiB_2 composite and pure Ti had a predominantly α-Ti phase microstructure, both as received and after processing. TiB whiskers are created when the Ti matrix reacts with TiB_2.
2. The findings of the indirect contact (cytotoxicity) assessment of both groups showed that there were no statistically significant differences in terms of cell viability. This demonstrated that the material's extract, which does not impair cell viability, may demonstrate the composite's cytocompatibility.
3. All the samples subjected to electrochemical tests revealed that these composite samples had stronger corrosion resistance than the pure samples.
4. The contact angle of the composite (44.29°) was lower than that of pure Ti (56.31°), indicating that the composite had a more hydrophilic surface and may have increased cell adhesion, with favorable osseointegration.
5. Based on the findings of this study and previous research, the titanium–titanium diboride (TI-TiB_2) composite shows promise as a biomaterial for dental implants or

other bone replacements due to its better corrosion resistance and wettability and good cytocompatibility.

6. Although the in vitro results showed that the Ti-TiB_2 composite would be a better choice as a biomaterial for dental implant applications, further in vivo studies are required to ensure its success in clinical applications.

Author Contributions: Conceptualization, A.M.A.A. and A.A.F.; methodology, A.M.A.A. and A.A.F.; validation, A.A.F. and J.H.; formal analysis, A.M.A.A., A.A.F. and J.H.; investigation, A.M.A.A.; resources, A.A.F.; data curation, A.M.A.A.; writing—original draft preparation, A.M.A.A. and A.A.F.; writing—review and editing, A.A.F. and J.H.; visualization, A.M.A.A. and J.H.; and supervision, A.A.F. and J.H. All authors have read and agreed to the published version of the manuscript.

Funding: This research received no external funding.

Data Availability Statement: The raw data supporting the conclusions of this article will be made available by the authors on request.

Conflicts of Interest: The authors declare no conflicts of interest.

References

1. Rosa, A.L.; Crippa, G.E.; de Oliveira, P.T.; Taba, M., Jr.; Lefebvre, L.P.; Beloti, M.M. Human alveolar bone cell proliferation, expression of osteoblastic phenotype, and matrix mineralization on porous titanium produced by powder metallurgy. *Clin. Oral Implant. Res.* **2009**, *20*, 472–481. [CrossRef] [PubMed]
2. Kadhim, D.R.; Hamad, T.I.; Fatalla, A.A. Use of Eggshells as Bone Grafts around Commercially Pure Titanium Implant Screws Coated with Nano Calcium Sulfate. *Int. J. Biomater.* **2022**, *2022*, 8722283. [CrossRef] [PubMed]
3. Bhattarai, S.R.; Khalil, K.A.; Dewidar, M.; Hwang, P.H.; Yi, H.K.; Kim, H.Y. Novel production method and in-vitro cell compatibility of porous Ti-6Al-4V alloy disk for hard tissue engineering. *J. Biomed. Mater. Res. Part A* **2008**, *86*, 289–299. [CrossRef] [PubMed]
4. Duraccio, D.; Mussano, F.; Faga, M.G. Biomaterials for dental implants: Current and future trends. *J. Mater. Sci.* **2015**, *50*, 4779–4812. [CrossRef]
5. Jani, G.H.; Fatalla, A.A. Characterization and Testing the properties of PEKK-Strontium-hydroxyapatite composite material. *Res. J. Pharm. Technol.* **2022**, *15*, 3034–3040. [CrossRef]
6. Jani, G.H.; Fatalla, A.A. Surface Characterization of PEKK Modified by stron-tium–hydroxyapatite coating as implant material Via the magnetron sputtering Deposition technique. *J. Baghdad Coll. Dent.* **2022**, *34*, 25–36. [CrossRef]
7. Mohammed, A.A.; Hamad, T.I. Assessment of Coating Zirconium Implant Material with Nanoparticles of Faujasite. *J. Baghdad Coll. Dent.* **2021**, *33*, 25–30. [CrossRef]
8. Powers, J.M.; Wataha, J.C. *Dental Materials-E-Book: Foundations and Applications*; Elsevier Health Sciences: Amsterdam, The Netherlands, 2015.
9. Kim, K.T.; Eo, M.Y.; Nguyen, T.T.H.; Kim, S.M. General review of titanium toxicity. *Int. J. Implant. Dent.* **2019**, *5*, 10. [CrossRef] [PubMed]
10. Whitters, C.J.; Strang, R.; Brown, D.; Clarke, R.L.; Curtis, R.V.; Hatton, P.V.; Ireland, A.J.; Lloyd, C.H.; McCabe, J.F.; Nicholson, J.W.; et al. Dental materials: 1997 literature review. *J. Dent.* **1999**, *27*, 401–435. [CrossRef]
11. Souza, J.C.; Ponthiaux, P.; Henriques, M.; Oliveira, R.; Teughels, W.; Celis, J.-P.; Rocha, L.A. Corrosion behaviour of titanium in the presence of Streptococcus mutans. *J. Dent.* **2013**, *41*, 528–534. [CrossRef]
12. Geurs, N.C.; Vassilopoulos, P.J.; Reddy, M.S.J.O.; Clinics, M.S. Soft tissue considerations in implant site development. *Surg. Clin. N. Am.* **2010**, *22*, 387–405. [CrossRef] [PubMed]
13. Grandin, H.M.; Berner, S.; Dard, M.J.M. A review of titanium zirconium (TiZr) alloys for use in endosseous dental implants. *Materials* **2012**, *5*, 1348–1360. [CrossRef]
14. Park, Y.-J.; Song, Y.-H.; An, J.-H.; Song, H.-J.; Anusavice, K.J. Cytocompatibility of pure metals and experimental binary titanium alloys for implant materials. *J. Dent.* **2013**, *41*, 1251–1258. [CrossRef] [PubMed]
15. Makau, F.; Morsi, K.; Gude, N.; Alvarez, R.; Sussman, M.; May-Newman, K. Viability of titanium-titanium boride composite as a biomaterial. *ISRN Biomater.* **2013**, *2013*, 970535. [CrossRef]
16. Morsi, K.; Patel, V.V. Processing and properties of titanium–titanium boride (TiBw) matrix composites—A review. *J. Mater. Sci.* **2007**, *42*, 2037–2047. [CrossRef]
17. Ammisetti, D.K.; Kruthiventi, S.H.H. Recent trends on titanium metal matrix composites: A review. *Mater. Today Proc.* **2021**, *46*, 9730–9735. [CrossRef]
18. Zhou, Y.; Yang, F.; Chen, C.; Shao, Y.; Lu, B.; Sui, Y.; Guo, Z. Mechanical property and microstructure of in-situ TiB/Ti composites via vacuum sintering and hot rolling. *J. Alloy. Compd.* **2022**, *911*, 165042. [CrossRef]
19. Xiang, T.; Ding, S.; Li, C.; Zheng, S.; Hu, W.; Wang, J.; Liu, P. Effect of current density on wettability and corrosion resistance of superhydrophobic nickel coating deposited on low carbon steel. *Mater. Des.* **2017**, *114*, 65–72. [CrossRef]

20. Thompson, S.W. Microstructural characterization of an as-quenched HSLA-100 plate steel via transmission electron microscopy. *Mater. Charact.* **2013**, *77*, 89–98. [CrossRef]
21. Ozerov, M.; Klimova, M.; Vyazmin, A.; Stepanov, N.; Zherebtsov, S. Orientation relationship in a Ti/TiB metal-matrix composite. *Mater. Lett.* **2017**, *186*, 168–170. [CrossRef]
22. Wang, T.; Gwalani, B.; Shukla, S.; Frank, M.; Mishra, R.S. Development of in situ composites via reactive friction stir processing of Ti–B4C system. *Mater. Lett.* **2019**, *172*, 54–60. [CrossRef]
23. Zehra, T.; Kaseem, M.; Hossain, S.; Ko, Y.-G. Fabrication of a protective hybrid coating composed of TiO_2, MoO_2, and SiO_2 by plasma electrolytic oxidation of titanium. *Metals* **2021**, *11*, 1182. [CrossRef]
24. Eriksson, M.; Salamon, D.; Nygren, M.; Shen, Z. Spark plasma sintering and deformation of Ti–TiB_2 composites. *Mater. Sci. Eng. A* **2008**, *475*, 101–104. [CrossRef]
25. Morsi, K.; Patel, V.; Naraghi, S.; Garay, J. Processing of titanium–titanium boride dual matrix composites. *J. Am. Acad. Dermatol.* **2008**, *196*, 236–242. [CrossRef]
26. Upadhyaya, G.J.; German, R.M. *Powder Metallurgy and Particulate Materials Processing*; Metal Powder Industries Federation: Princeton, NJ, USA, 2005; p. 522. ISBN 0-9762057-1-8.
27. Selvakumar, M.; Chandrasekar, P.; Mohanraj, M.; Ravisankar, B.; Balaraju, J. Role of powder metallurgical processing and TiB reinforcement on mechanical response of Ti–TiB composites. *Mater. Lett.* **2015**, *144*, 58–61. [CrossRef]
28. Patel, V.; El-Desouky, A.; Garay, J.; Morsi, K. Pressure-less and current-activated pressure-assisted sintering of titanium dual matrix composites: Effect of reinforcement particle size. *Mater. Sci. Eng. A* **2009**, *507*, 161–166. [CrossRef]
29. Gaisin, R.A.; Imayev, V.M.; Imayev, R.M. Effect of hot forging on microstructure and mechanical properties of near α titanium alloy/TiB composites produced by casting. *J. Alloy. Compd.* **2017**, *723*, 385–394. [CrossRef]
30. Lu, H.; Zhang, D.; Gabbitas, B.; Yang, F.; Matthews, S. Synthesis of a TiBw/Ti6Al4V composite by powder compact extrusion using a blended powder mixture. *J. Alloy. Compd.* **2014**, *606*, 262–268. [CrossRef]
31. Xiang, J.; Han, Y.; Li, J.; Qiu, P.; Sun, X.; Lu, W. Microstructure characteristics of ECAP-processed (TiB+ La_2O_3)/Ti-6Al-4V composites. *J. Alloys Compd.* **2017**, *726*, 57–66. [CrossRef]
32. Guo, X.; Lu, W.; Wang, L.; Qin, J. A research on the creep properties of titanium matrix composites rolled with different deformation degrees. *Mater. Des.* **2014**, *63*, 50–55. [CrossRef]
33. Attar, H.; Ehtemam-Haghighi, S.; Kent, D.; Dargusch, M.S. Recent developments and opportunities in additive manufacturing of titanium-based matrix composites: A review. *Int. J. Mach. Tools Manuf.* **2018**, *133*, 85–102. [CrossRef]
34. Morsi, K. Titanium–titanium boride composites. *J. Mater. Sci.* **2019**, *54*, 6753–6771. [CrossRef]
35. Einarsrud, M.; Hagen, E.; Pettersen, G.; Grande, T. Pressureless sintering of titanium diboride with nickel, nickel boride, and iron additives. *J. Am. Ceram. Soc.* **1997**, *80*, 3013–3020. [CrossRef]
36. Panda, K.B.; Chandran, K.S.R. Synthesis of ductile titanium-titanium boride (Ti-TiB) composites with a beta-titanium matrix: The nature of TiB formation and composite properties. *Met. Mater. Trans. A* **2003**, *34*, 1371–1385. [CrossRef]
37. Asl, M.S.; Namini, A.S.; Motallebzadeh, A.; Azadbeh, M. Effects of sintering temperature on microstructure and mechanical properties of spark plasma sintered titanium. *Mater. Chem. Phys.* **2018**, *203*, 266–273.
38. Ozerov, M.; Klimova, M.; Kolesnikov, A.; Stepanov, N.; Zherebtsov, S. Deformation behavior and microstructure evolution of a Ti/TiB metal-matrix composite during high-temperature compression tests. *Mater. Des.* **2016**, *112*, 17–26. [CrossRef]
39. Sabahi Namini, A.; Azadbeh, M. Microstructural characterisation and mechanical properties of spark plasma-sintered TiB2-reinforced titanium matrix composite. *Powder Metall.* **2017**, *60*, 22–32. [CrossRef]
40. Ozerov, M.; Stepanov, N.; Kolesnikov, A.; Sokolovsky, V.; Zherebtsov, S. Brittle-to-ductile transition in a Ti–TiB metal-matrix composite. *Mater. Lett.* **2017**, *187*, 28–31. [CrossRef]
41. Sergi, A.; Khan, R.H.; Irukuvarghula, S.; Meisnar, M.; Makaya, A.; Attallah, M.M. Development of Ni-base metal matrix composites by powder metallurgy hot isostatic pressing for space applications. *Adv. Powder Technol.* **2022**, *33*, 103411. [CrossRef]
42. Ogawa, T.J.O. Ultraviolet photofunctionalization of titanium implants. *Oral Craniofacial Tissue Eng.* **2012**, *2*, 151. [CrossRef]
43. Kim, S.-P.; Kaseem, M.; Choe, H.-C. Plasma electrolytic oxidation of Ti-25Nb-xTa alloys in solution containing Ca and P ions. *Surf. Coat. Technol.* **2020**, *395*, 125916. [CrossRef]
44. Zhang, B.; Yang, Y.; Fan, X. Processing, microstructure, and properties of porous ceramic composites with directional channels. *J. Mater. Sci. Technol.* **2024**, *168*, 1–15. [CrossRef]
45. Kumar, M.S.; Chandrasekar, P.; Chandramohan, P.; Mohanraj, M. Characterisation of titanium–titanium boride composites processed by powder metallurgy techniques. *Mater. Charact.* **2012**, *73*, 43–51. [CrossRef]
46. *ISO 10993-5:2009*; Biological Evaluation of Medicaldevices, Part 5: Tests for In Vitro Cytotoxicity. ISO: Geneva, Switzerland, 2009.
47. *ASTM F746-04*; Standard Test Method for Pitting or Crevice Corrosion of Metallic Surgical Implant Materials. ASTM International: West Conshohocken, PA, USA, 2014.
48. *ASTM D7334-08*; Standard Practice for Surface Wettability of Coatings, Substrates and Pigments by Advancing contact angle Measurement. ASTM International: West Conshohocken, PA, USA, 2013.
49. Golla, B.R.; Bhandari, T.; Mukhopadhyay, A.; Basu, B. Titanium diboride. In *Ultra-High Temperature Ceramics: Materials for Extreme Environment Applications*; American Ceramic Society: Columbus, OH, USA, 2014; pp. 316–360.
50. Maseko, S.; Popoola, A.; Fayomi, O. Characterization of ceramic reinforced titanium matrix composites fabricated by spark plasma sintering for anti-ballistic applications. *Def. Technol.* **2018**, *14*, 408–411. [CrossRef]

51. Mejía-Caballero, I.; Palomar-Pardavé, M.; Trinidad, J.M.; Romero-Romo, M.; Pasten-Borja, R.P.; Lartundo-Rojas, L.; López-García, C.; Campos-Silva, I. Corrosion behavior of AISI 316 L borided and non-borided steels immersed in a simulated body fluid solution. *Surf. Coatings Technol.* **2015**, *280*, 384–395. [CrossRef]
52. Campos-Silva, I.; Palomar-Pardavé, M.; Pastén-Borja, R.P.; Feridun, O.K.; Bravo-Bárcenas, D.; López-García, C.; Reyes-Helguera, R. Tribocorrosion and cytotoxicity of FeB-Fe_2B layers on AISI 316 L steel. *Surf. Coat. Technol.* **2018**, *349*, 986–997. [CrossRef]
53. Peng, T.-Y.; Shih, Y.-H.; Hsia, S.-M.; Wang, T.-H.; Li, P.-J.; Lin, D.-J.; Sun, K.-T.; Chiu, K.-C.; Shieh, T.-M. In vitro assessment of the cell metabolic activity, cytotoxicity, cell attachment, and inflammatory reaction of human oral fibroblasts on polyetheretherketone (PEEK) implant–abutment. *Polymers* **2021**, *13*, 2995. [CrossRef]
54. Dai, Y.; Jiang, X.; Ou, M.; Li, K.; Xiang, Q.; Yang, F.; Liu, J. Tribocorrosion Behaviour of a Ti–25Nb–3Zr–2Sn–3Mo Alloys Induction Nitride Layer in a Simulated Body Fluid Solution. *Coatings* **2023**, *13*, 231. [CrossRef]
55. Niinomi, M. *Metals for Biomedical Devices*; Woodhead Publishing: Sawston, UK, 2019.
56. Liu, L.; Meng, Y.; Volinsky, A.A.; Zhang, H.-J.; Wang, L.-N. Influences of albumin on in vitro corrosion of pure Zn in artificial plasma. *Corros. Sci.* **2019**, *153*, 341–356. [CrossRef]
57. Scully, J.R.; Budiansky, N.D.; Tiwary, Y.; Mikhailov, A.S.; Hudson, J.L. An alternate explanation for the abrupt current increase at the pitting potential. *Corros. Sci.* **2008**, *50*, 316–324. [CrossRef]
58. Craciun, D.; Laszlo, E.A.; Mirza-Rosca, J.C.; Dorcioman, G.; Geanta, V.; Voiculescu, I.; Craciun, G.; Badea, L.; Craciun, V. Structural Parameters and Behavior in Simulated Body Fluid of High Entropy Alloy Thin Films. *Materials* **2024**, *17*, 1162. [CrossRef] [PubMed]
59. Al-Radha, A.S.D.; Dymock, D.; Younes, C.; O'Sullivan, D. Surface properties of titanium and zirconia dental implant materials and their effect on bacterial adhesion. *J. Dent.* **2012**, *40*, 146–153. [CrossRef] [PubMed]
60. Lucca, G.d.S.D.; Daleffe, A.; Scheffer, G.S.; de Souza, M.A.; Marques, C.R.; Castelan, J.; Schaeffer, L. Investigation of wettability using contact angle measurements and geometric discrepancy analysis of heat-treated pure titanium grade 2. *Mater. Res.* **2021**, *24*, e20210102. [CrossRef]
61. Sahay, S.S.; Ravichandran, K.S.; Atri, R.; Chen, B.; Rubin, J. Evolution of microstructure and phases in in situ processed Ti–TiB composites containing high volume fractions of TiB whiskers. *J. Mater. Res.* **1999**, *14*, 4214–4223. [CrossRef]
62. Kim, M.G.; Sung, S.Y.; Kim, Y.J. (Eds.) *Synthesis of In-Situ Titanium Carbide Particle Reinforced Titanium Composites*; Materials Science Forum; Trans Tech Publications Ltd.: Bäch, Switzerland, 2005.
63. *ASTM E407-07*; Standard Practice for Microetching Metals and Alloys. ASTM International: West Conshohocken, PA, USA, 2011.
64. Gammon, L.M.; Briggs, R.D.; Packard, J.M.; Batson, K.W.; Boyer, R.; Domby, C.W. Metallography and microstructures of titanium and its alloys. In *ASM Handbook Metallography and Microstructures*; ASTM International: West Conshohocken, PA, USA, 2004; Volume 9, pp. 899–917.
65. Türkez, H.; Arslan, M.E.; Tatar, A.; Özdemir, Ö.; Sönmez, E.; Çadirci, K.; Hacimüftüoğlu, A.; Ceylan, B.; Açikyildiz, M.; Kahraman, C.Y.; et al. Molecular Genetics and Cytotoxic Responses to Titanium Diboride and Zinc Borate Nanoparticles on Cultured Human Primary Alveolar Epithelial Cells. *Materials* **2022**, *15*, 2359. [CrossRef]
66. Fanton, L.; Loria, F.; Amores, M.; Pazos, M.R.; Adán, C.; García-Muñoz, R.A.; Marugán, J. Proliferation of osteoblast precursor cells on the surface of TiO2 nanowires anodically grown on a β-type biomedical titanium alloy. *Sci. Rep.* **2022**, *12*, 7895. [CrossRef]
67. Vijayalakshmi, U.; Chellappa, M.; Anjaneyulu, U.; Manivasagam, G. Preparation and evaluation of the cytotoxic nature of TiO_2 nanoparticles by direct contact method. *Int. J. Nanomed.* **2015**, *10* (Suppl. S2), 31–41. [CrossRef] [PubMed]
68. Ellakany, P.; AlGhamdi, M.A.; Alshehri, T.; Abdelrahman, Z.; Alshehri Sr, T.A. Cytotoxicity of commercially pure titanium (cpTi), silver-palladium (Ag-Pd), and nickel-chromium (Ni-Cr) alloys commonly used in the fabrication of dental prosthetic restorations. *Cureus* **2022**, *14*, e31679. [CrossRef]
69. Al-Murshdy, J.M.S.; Al-Deen, H.H.J.; Hussein, S.R. Investigation of the effect of indium addition on the mechanical and electrochemical properties of the Ti–15Mo biomedical alloy. *J. Bio- Tribo-Corros.* **2021**, *7*, 148. [CrossRef]
70. Kaseem, M.; Zehra, T.; Khan, M.A.; Safira, A.R.; Cho, H.; Lee, J.; Lee, G.; Yang, H.W.; Park, N. Guar gum-driven high-energy plasma electrolytic oxidation for concurrent improvements in the electrochemical and catalytic properties of Ti-15 Zr alloy. *Surf. Interfaces* **2022**, *34*, 102403. [CrossRef]
71. Kaseem, M.; Choe, H.-C. The effect of in-situ reactive incorporation of MoOx on the corrosion behavior of Ti-6Al-4 V alloy coated via micro-arc oxidation coating. *Corros. Sci.* **2021**, *192*, 109764. [CrossRef]
72. Koç, E. Corrosion behaviour of as cast β-Mg17Al12 phase in 3.5 wt% NaCl solution. *Acta Phys. Pol. A* **2019**, *135*, 881. [CrossRef]
73. Putz, B. The Influence of High Current Densities on Intact and Cracked Thin Gold Films on Flexible Polyimide Substrate. Diploma Thesis, University of Leoben, Leoben, Austria, 2014.
74. Hansen, D.C. Metal corrosion in the human body: The ultimate bio-corrosion scenario. *Electrochem. Soc. Interface* **2008**, *17*, 31. [CrossRef]
75. Le Guéhennec, L.; Soueidan, A.; Layrolle, P.; Amouriq, Y. Surface treatments of titanium dental implants for rapid osseointegration. *Dent. Mater.* **2007**, *23*, 844–854. [CrossRef]
76. Barbosa, T.P.; Naves, M.M.; Menezes, H.H.M.; Pinto, P.H.C.; de Mello, J.D.B.; Costa, H.L. Topography and surface energy of dental implants: A methodological approach. *J. Braz. Soc. Mech. Sci. Eng.* **2017**, *39*, 1895–1907. [CrossRef]

77. Lauria, I.; Kutz, T.N.; Böke, F.; Rütten, S.; Zander, D.; Fischer, H. Influence of nanoporous titanium niobium alloy surfaces produced via hydrogen peroxide oxidative etching on the osteogenic differentiation of human mesenchymal stromal cells. *Mater. Sci. Eng. C* **2019**, *98*, 635–648. [CrossRef]
78. Roach, P.; Shirtcliffe, N.J.; Newton, M.I. Progess in superhydrophobic surface development. *Soft Matter* **2008**, *4*, 224–240. [CrossRef]
79. Xi, L. High-Temperature Interactions of Molten Ti-Al, Ni-Al and Ni-B Alloys with TiB_2 Ceramic. Ph.D. Dissertation, Technische Universität Dresden, Dresden, Germany, 2017.
80. Aljafery, A.M.A.; Fatalla, A.A.; Haider, J. Powder metallurgy preparation and characterization of titanium-titanium diboride composite targeted for dental implant. *J. Compos. Sci.* **2023**, *7*, 353. [CrossRef]
81. Cervino, G.; Fiorillo, L.; Iannello, G.; Santonocito, D.; Risitano, G.; Cicciù, M. Sandblasted and acid etched titanium dental implant surfaces systematic review and confocal microscopy evaluation. *Materials* **2019**, *12*, 1763. [CrossRef]
82. Maître, J.-L.; Heisenberg, C.-P. The role of adhesion energy in controlling cell–cell contacts. *Curr. Opin. Cell Biol.* **2011**, *23*, 508–514. [CrossRef]
83. dos Santos Monteiro, E.; de Souza Soares, F.M.; Nunes, L.F.; Santana, A.I.C.; de Biasi, R.S.; Elias, C.N.J. Comparison of the wettability and corrosion resistance of two biomedical Ti alloys free of toxic elements with those of the commercial ASTM F136 (Ti–6Al–4V) alloy. *J. Mater. Res. Technol.* **2020**, *9*, 16329–16338. [CrossRef]